MATERIALS SCIENCE

Wavelength-tunable and shape-reconfigurable photonic capsule resonators containing cholesteric liquid crystals

Sang Seok Lee[1], Jong Bin Kim[1], Yun Ho Kim[2], Shin-Hyun Kim[1]*

Cholesteric liquid crystals (CLCs) have a photonic bandgap due to the periodic change of refractive index along their helical axes. The CLCs containing optical gain have served as band-edge lasing resonators. In particular, CLCs in a granular format provide omnidirectional lasing, which are promising as a point light source. However, there is no platform that simultaneously achieves high stability in air and wavelength tunability. We encapsulate CLCs with double shells to design a capsule-type laser resonator. The fluidic CLCs are fully enclosed by an aqueous inner shell that promotes the planar alignment of LC molecules along the interface. The outer shell made of silicone elastomer protects the CLC core and the inner shell from the surroundings. Therefore, the helical axes of the CLCs are radially oriented within the capsules, which provide a stable omnidirectional lasing in the air. At the same time, the fluidic CLCs enable the fine-tuning of lasing wavelength with temperature. The capsules retain their double-shell structure during the dynamic deformation. Therefore, the CLCs in the core maintain the planar alignment along the deformed interface, and a lasing direction can be varied from omnidirectional to bi- or multidirectional, depending on the shape of deformed capsules.

INTRODUCTION

Liquid crystals (LCs) spontaneously form a cholesteric phase with a helical order when chiral dopants cause the orientation of nematic LC molecules regularly rotated along axes. As the refractive index is periodically modulated along the helical axes between extraordinary ($n_{\parallel}$) and ordinary ($n_{\perp}$) values, the cholesteric LCs (CLCs) have a photonic bandgap property (*1*, *2*). In a photonic stop band, a circularly polarized light of the same handedness to the CLC structure is selectively reflected due to low-photon density of states (DOS) (*3*). The photon DOS sharply increases in band edges, which enables the use of CLCs as mirrorless laser resonators (*4*, *5*). When light emitters, such as fluorescent dyes and quantum dots, are present in the CLCs, their emission spectra are markedly modulated. The emission at the stop band is significantly suppressed due to the low DOS, whereas the emission at band edges is greatly enhanced due to high DOS (*6*, *7*). In addition, a slow photon effect in band edges markedly increases the dwell time of photons in CLCs, enabling the stimulated emission (*8*, *9*). As the position of band edges is adjustable with external stimuli, so is the wavelength of lasing (*10*–*15*). In addition, the size of the laser resonator can be reduced to tens of micrometers as mirrors are not required in CLC band-edge lasers.

The direction of lasing emission is dictated by that of helical axes of CLCs. In a typical film format, the CLCs have a planar alignment along the entire planar surface so that they bidirectionally emit the laser (*16*–*18*). When the CLCs are tailored to have a granular format with spherical symmetry, the helical axes are radially organized due to planar alignment along the spherical surface, which leads to omnidirectional lasing (*19*–*21*). The omnidirectional lasing is potentially important for three-dimensional scanning or imaging (*22*–*24*). The omnidirectional lasers have been implemented by forming CLC emulsion drops dispersed in water (*19*–*21*). Although surfactants stabilized the emulsion interface, the aqueous surrounding is a prerequisite to maintain spherical compartment of CLC drops. To make the omnidirectional CLC resonators stable in an air environment, the CLC drops are solidified by polymerizing reactive mesogen (*25*). However, the solid CLC microspheres lose wavelength tunability, instead of securing air stability. It remains an important challenge to produce omnidirectional lasers with high air stability and wavelength tunability. In addition, it will be highly beneficial for various applications to make the resonators controllable over lasing direction and intensity.

Here, we design a CLC resonator in a capsule format to simultaneously achieve high air stability, wavelength and intensity tunability, and lasing-direction controllability. The capsule resonators have a triple-layered structure, which comprises a CLC core, an ultrathin alignment shell, and a thick elastic solid shell. The capsules are microfluidically created to have uniform size and composition by using oil-in-water-in-oil-in-water (O/W/O/W) triple-emulsion drops as a template. The innermost oil is a liquid CLC containing a fluorescent dye, the inner water shell is an aqueous solution of poly(vinyl alcohol) (PVA) and glycerol, and the outer oil shell is a photocross-linkable silicone precursor. The nonvolatile PVA and glycerol in the inner shell induce and maintain a planar alignment of the CLC molecules along the interface of the core even if water evaporates in an air environment. The silicone elastomer shell formed by photocross-linking provides the shape reconfigurability and high mechanical stability of the capsule structure. Therefore, the CLC capsules enable a stable omnidirectional lasing in an air environment. At the same time, the fluidic CLC core provides wavelength tunability along with an external stimulus of temperature. As the elastic shell allows reversible deformation of the capsules from spherical to nonspherical shapes while maintaining a planar alignment, the lasing direction can be adjusted from the omnidirectional to bi- or multidirectional. Consequently, one can control the intensity of laser on the target location by adjusting the degree and shape of the deformation.

[1]Department of Chemical and Biomolecular Engineering (BK21 Plus Program), Korea Advanced Institute of Science and Technology, Daejeon 34141, Republic of Korea. [2]Advanced Materials Division, Korea Research Institute of Chemical Technology, Daejeon 34114, Republic of Korea.
*Corresponding author. Email: kim.sh@kaist.ac.kr

RESULTS

Microfluidic production of air-stable CLC capsules

A helical structure of CLCs provides a photonic bandgap property, which has been used as a mirrorless laser resonator at band-edge mode. To create CLC lasers with a capsule format, we encapsulate a dye-dissolved CLC solution with double shells (Fig. 1A). The inner shell is an aqueous layer for planar LC alignment, and the outer shell is an elastomeric solid membrane for protection of the encapsulants (*26*). The capsules are produced by using O/W/O/W triple-emulsion drops as a template. To prepare highly uniform droplets in composition and size, we use a capillary microfluidic device (fig. S1). The capillary microfluidic device consists of two tapered cylindrical capillaries assembled in a square capillary. One tapered capillary has a hydrophilic inner wall and a hydrophobic outer wall, and the other has hydrophilic walls only.

To compose a CLC laser resonator in the core of capsules, we mixed an LC (E7) with a chiral dopant (R5011) and a fluorescent dye [PM597 (1,3,5,7,8-pentamethyl-2,6-di-t-butylpyrromethene-difluoroborate complex)], which we used as an innermost oil phase. As a middle water phase to form an alignment layer, we used an aqueous solution of 12% (w/w) of PVA and 7% (w/w) of glycerol, which stabilize the oil-water interface and promote planar alignment of LC molecules (*27*). To make the outer elastic shell, we used a photocurable silicone methacrylate as the outer oil phase. We used a 10% (w/w) aqueous solution of PVA as a continuous phase. We simultaneously injected the innermost CLC solution and an aqueous solution of PVA and glycerol through the tapered capillary with a hydrophilic inner wall. Because of the hydrophilic surface, the CLC forms a train of plug-shaped drops in the aqueous solution, which flows the capillary without contacting the inner wall. This discontinuous core-sheath flow and a photocurable silicone methacrylate flowing along the outer wall are simultaneously emulsified into the continuous phase that is injected along the outer wall of the other tapered capillary as a counterflow. As a result, O/W/O/W droplets are formed at the tip-to-tip junction, which flow through the inner channel of the hydrophilic tapered capillary. Because the core-sheath flow is discontinuous, the triple-emulsion drops and CLC core-free W/O/W double-emulsion drops are cyclically produced. Nevertheless, the triple-emulsion drops are selectively collected from the double-emulsion drops by exploiting their density difference (*26*). The triple-emulsion drops are exposed to ultraviolet (UV) light to polymerize the silicon methacrylate in the outer shell and then stored for 1 day to fully induce planar alignment of CLCs.

The capsules are highly monodisperse and stable. The thicknesses of the inner and outer shells are typically 2 and 23 μm, respectively. The capsules immersed in shallow water show a unique color pattern that is composed of a bright central dot and two series of dots along two circles with different polar angles (fig. S2); one series of dots disappears when the level of water is high. The central dot is caused by normal reflection of light, and the series of dots are developed from photonic cross-communications between neighboring capsules (see fig. S2 for the detailed light paths) (*28*, *29*). These color patterns indirectly indicate that the CLC in the capsule has a radial configuration of the helical axes as LC molecules take a planar alignment along the spherical interface of the core (*30*). When the capsules are dried in air, they form hexagonal arrays while maintaining spherical shape (Fig. 1, B and C). Each capsule in the array also shows a unique color pattern featured by a bright central dot and a series of several dots along the circle with a polar angle of 45°. This implies that the helical axis of CLC in the capsule maintains a radial

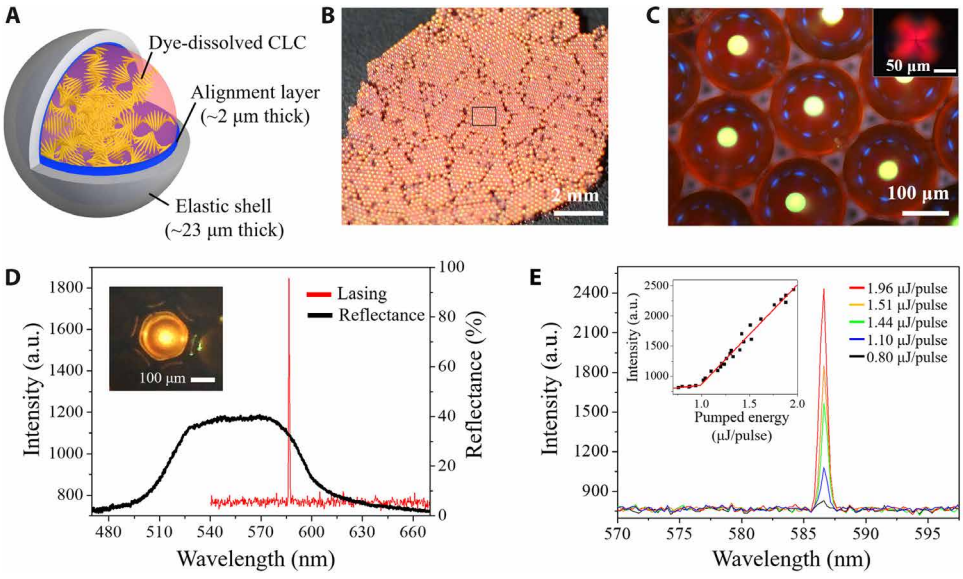

Fig. 1. Air-stable CLC capsule resonators. (**A**) Schematic of a photonic capsule resonator composed of a dye-dissolved CLC core, an inner alignment layer, and an outer elastic shell. (**B** and **C**) Photograph and optical microscopy (OM) image of dried CLC capsules taken in reflection mode without polarization. The capsules maintain their spherical shape and radially aligned helical axes in the air, which results in photonic cross-communication. The inset of (C) is a cross-polarized OM image in transmission mode, which shows small and large fourfold patterns at the center. (**D**) Reflectance spectrum (right *y* axis) of CLC capsules in the air and lasing spectrum (left *y* axis) in the LWE on the CLC capsules. We obtained the reflectance spectrum by subtracting the spectrum taken at 60°C (isotropic state) from the measured one to exclude the influence of the dye absorption. The inset shows a lasing on the capsules. (**E**) Series of the emission spectra on the capsules in the air at various pumped energies. The inset shows an emission intensity as a function of the pumped energy, which has a threshold value of 0.98 μJ per pulse.

configuration even in the air. The dried capsule shows small and large fourfold patterns at the centermost in cross-polarized optical microscopy at transmission mode (Fig. 1C, inset), which further proves the radial configuration (*31*). Although water in the inner shell slowly evaporates through the outer shell, nonvolatile glycerol and PVA remain in the shell and help CLC retain the planar alignment along the interface; the complete evaporation of water yields a 400-nm-thick layer. The fractional volume reduction to the entire core is as small as 5.8%, which does not cause buckling or shape deformation.

Lasing from CLC capsules

We set the concentration of a chiral dopant (R5011) to 2.64% (w/w) to locate the long-wavelength edge (LWE) of the stop band in the spontaneous emission spectrum of the fluorescent dye (PM597), where we set the concentration of the dye to 0.5% (w/w). The capsule shows a stop band centered at a wavelength of 555 nm and an LWE of around 583 nm (Fig. 1D). When the capsule is optically pumped by a frequency-doubled Q-switched neodymium-doped yttrium-aluminum-garnet (Nd:YAG) laser emitting 4-ns pulses at a wavelength of 532 nm, with a repetition rate of 1 Hz and a beam diameter of 800 μm, we detected a strong and sharp emission at 586.6 nm, distinguished from the spontaneous emission (see fig. S3 for the detailed optical setup).

The energy of the pumping source influences the lasing spectra of the capsule (Fig. 1E). With a pumped energy of 0.80 μJ per pulse, we observed no sharp emission peak. When the energy is increased to 1.10 μJ per pulse, we detected a sharp emission at the wavelength of 586.6 nm, and the intensity increases along with the pumped energy. The intensity of the emission shows a typical threshold behavior (Fig. 1E, inset). The emission intensity slowly increases with the pumped energy below 0.98 μJ per pulse, whereas it steeply increases above 0.98 μJ per pulse; the slope above the threshold is one order of magnitude larger than that below the threshold. A full width at half maximum (FWHM) is as small as 0.61 nm, and the *Q*-factor ($\lambda/\Delta\lambda$) is 960. This lasing performance is comparable with CLCs in film format, indicating that the CLCs confined in the spherical capsules have a high quality of LC alignment (*18*, *32*).

Control of lasing wavelength with temperature

The CLC core remains fluidic so that the band edges are tunable to external stimuli. To render the CLC temperature-sensitive in the range of 18° to 34°C, we formulate the core solution to have 0.68% (w/w) of R5011 and 19.8% (w/w) of R811. The chiral dopant R5011 is insensitive to a temperature below 50°C, whereas the chiral dopant R811 is highly sensitive in the range of 10° to 40°C (*33*, *34*); the mechanism by which the stop band shifts along with temperature is known as the temperature-dependent solubility and twisting power of the dopant (*35*). This specific composition of the CLC solution has a central stop band at 669 nm at 18°C, which shifts to 539 nm at 34°C (fig. S4). As a short-wavelength edge (SWE) or LWE is overlapped with a spontaneous emission spectrum of the dye in the range of the stop-band shift, we expect the lasing wavelength to be tunable by temperature in the entire range of 18° to 34°C.

The CLC capsule changes from red to green as the temperature increases from 18° to 34°C (Fig. 2A), which is consistent with the temperature-dependent stop-band shift. The lasing wavelength from the capsule also depends on the temperature (Fig. 2, B and C). In the range of temperature of 18° to 21.5°C, lasing occurs in an SWE (Fig. 2B). This is because the SWE is overlapped with the spontaneous emission spectrum of the dye, whereas the LWE is not overlapped or overlapped at the very low intensity. By contrast, lasing occurs in LWE above 22°C (Fig. 2C). Note that the intensity of spontaneous emission of the dye in SWE is much larger than that in LWE at 22°C (Fig. 2D and fig. S4). Nevertheless, LWE is selected for lasing when the pumped energy is lower than 4 μJ per pulse. This is due to a preferential alignment of the transition dipole moment of the dye molecule PM597. The order parameter of the transition dipole moment of the dye in a host LC (E7) is approximately 0.38, implying that the dye preferentially emits parallel to the director of the LC molecules (*36*, *37*). Therefore, we expect a high rate of emission in LWE, which is related to the extraordinary refractive index ($n_{\parallel}$), rather than in SWE, which is related to ordinary index ($n_{\perp}$) (*16*, *38*). When the pumping energy exceeds 4.25 μJ per pulse, we also observed lasing in SWE at 22°C (fig. S5). The threshold in SWE is much higher than that in LWE (1.05 μJ per pulse).

Figure 2D summarizes the overall temperature-dependent shifts of lasing wavelength. The wavelength in SWE shifts from 613.0 to 565.3 nm along with the temperature in the range of 18° to 21.5°C, with an average slope of −14.0 nm/°C, whereas that in LWE shifts from 621.7 to 563.2 nm in the range of 22° to 34°C, with an average slope of −4.80 nm/°C. The threshold values in SWE and LWE are inversely proportional to the spontaneous emission intensity of the dye (Fig. 2E and fig. S6). There is no meaningful difference in the threshold value between LWE and SWE when the only single edge is predominantly overlapped with the emission spectrum. Therefore, we suggest controlling the lasing wavelength with a temperature in the range of 22° to 34°C in LWE as LWE provides more precise control than SWE due to the low slope.

Control of lasing direction and intensity

The spherical CLC capsules show omnidirectional lasing as the helical axes of CLC are radially oriented. The capsules can be elastically deformed under mechanical stress to control the lasing direction. When compressed by a pair of glass plates, the capsule is transformed from a sphere to a disk (Fig. 3, A and B). The elastic outer shell deforms to fit into the confinement during the compression while maintaining the integrity. The inner liquid shell for planar alignment also maintains the integrity during the deformation of capsules for the range of the flattening ratio (FR), 0 to 0.34; the FR is defined as the difference between the diameter and the height relative to the diameter of the deformed capsule (FR = 1 − *H*/*D*). This high stability of the inner liquid shell is attributed to the high lubrication resistance of the thin liquid film (*39*). Therefore, the alignment layer fully encloses the LC molecules in the core without directly contacting the outer shell during reversible and repeatable deformation. As a result, LC molecules retain a planar alignment along the interface of core, and helical axes are reorganized to align perpendicular to the flattened top and bottom surfaces. We observed a large fourfold pattern under cross-polarized optical microscopy, which elongates along the lateral direction during the deformation until FR = 0.45 (Fig. 3B). A small fourfold pattern in the centermost of spherical capsule gradually turns to a thick line defect. For larger deformation with FR > 0.60, CLC in the core shows no well-defined texture as the planar alignment of LC molecules along the interface is not able to immediately alter the arrangement of molecules in the middle. In addition, oily streaks are formed immediately after the deformation. The oily streaks

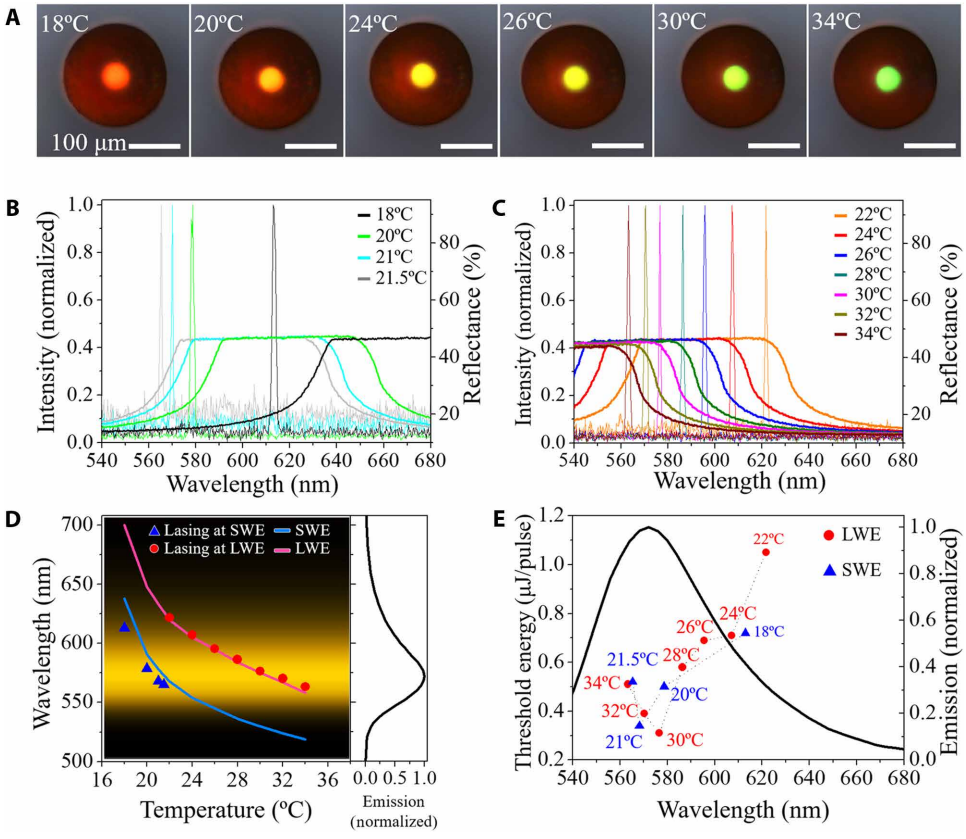

Fig. 2. Wavelength tuning with temperature. (**A**) Series of OM images of a CLC capsule taken at denoted temperatures. The stop band of CLC blue-shifts along with temperature. (**B** and **C**) Reflectance spectra (right *y* axis) of dye-free CLC film and lasing spectra (left *y* axis) from the capsules containing dye-dissolved CLC, where we used the same concentration of chiral dopants in the film and capsule. Lasing occurs in the SWE in the range of 18° to 21.5°C and occurs in the LWE in the range of 22° to 34°C. (**D**) Wavelengths of LWE, SWE, and lasing emission as a function of temperature, where a spontaneous emission spectrum of the dye is shown in the right panel and represented with a color gradient in the main panel. (**E**) Threshold energy (left *y* axis) for lasing on the CLC capsule in LWE (red circles) and SWE (blue triangles) as a function of wavelength. The temperature is also denoted. The spontaneous emission spectrum of the dye (right *y* axis) is shown for a comparison.

and the defects are gradually reduced as LC molecules spontaneously rearrange in the deformed capsule (movie S1). It takes approximately 1 hour to heal the oily streaks.

The compression of the capsule with a pair of the glass plates and subsequent rearrangement of CLC in the core lead to the expansion of the area responsible for strong reflection at the stop band (Fig. 3C). As the lasing occurs along the helical axes of CLC, one can tune the lasing direction from omnidirectional to mainly bidirectional by the deformation. Therefore, we can increase the intensity of the laser to the surface normal along with the degree of deformation (Fig. 3D); we incubated the deformed capsules in water for 1 hour before the measurement and subjected a single capsule to the optical pumping. As we increase the value of FR from 0 to 0.07, 0.14, 0.30, and 0.56, the output intensity markedly increases. For example, with a pumping energy of 1.4 μJ per pulse, the output intensities are 1.86, 3.30, 8.89, and 19.3 times larger than that at FR = 0. In addition, the output intensity relative to the pumping energy is increased in factors of 4.5, 6.4, 14.7, and 35.8, respectively.

To compare the structural quality of capsule resonators with different FRs, we normalize the output intensity with the input energy on the flattened top surface for each capsule. We calculate the input energy by considering a Gaussian intensity distribution of the pumping source with a spot diameter of 800 μm and the area of the flattened top surface (fig. S7). The input energy at FRs of 0.07, 0.14, 0.30, and 0.56 are 2.00, 3.54, 8.59, and 20.9 times larger than that at FR = 0. The output intensity normalized by the input energy is almost invariant for all FRs. For example, the values at various FRs relative to that at FR = 0 are in the range of 0.92 to 1.03 with a pumping energy of 1.4 μJ per pulse (Fig. 3E). This consistent output intensity indicates that the CLC in the core of the capsule maintains a comparable quality of laser resonators for the deformation with FR < 0.56. We can further confirm the maintenance of resonator quality from the consistent FWHM of the emission for all FRs (Fig. 3E).

Upon the deformation of the capsule, CLC instantly changes the shape while maintaining the planar alignment along the interface. However, it takes time to heal defects and oily streaks through the rearrangement in the middle. Therefore, the quality of laser emission is also enhanced over incubation time. Immediately after the deformation, we obtained relatively low intensity and slightly large FWHMs (fig. S8). The lasing intensity increases and reaches a plateau in 60 min at which intensity is almost doubled. The FWHM of the laser emission is 0.81 nm immediately after the deformation, which decreases to 0.68 nm in 40 min. We can dynamically tune the lasing direction by deforming the capsules, although the quality of laser is slightly lowered. To achieve a full performance of lasing, we require to incubate the capsule for 1 hour after the deformation.

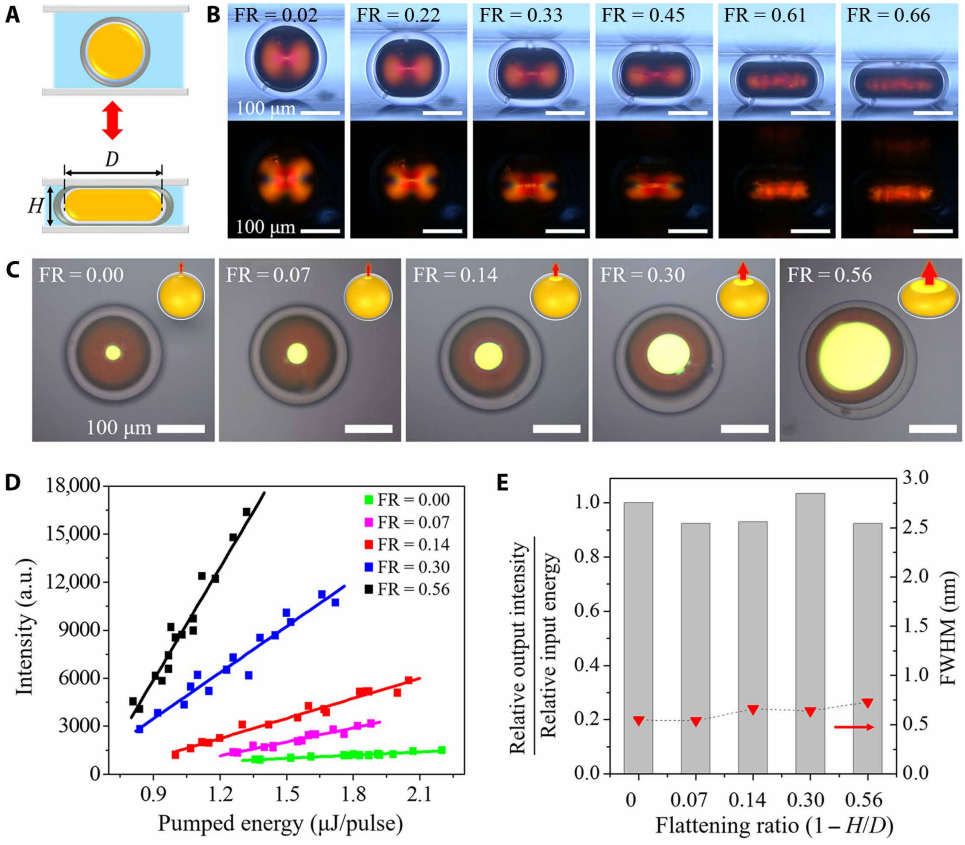

Fig. 3. Control of lasing direction and intensity. (**A**) Side view of the CLC capsule compressed by a pair of two plates. An FR of the deformed capsule is defined as FR = 1 − *H*/*D*. (**B**) Side-view OM images of a CLC capsule immediately after the deformation taken in transmission mode without polarization (top) and with cross-polarization (bottom). (**C**) Top-view OM images of a CLC capsule taken in reflection mode, showing the expansion of flattened area responsible for strong reflection at stop band, where FR is varied in the range of 0 to 0.56. The insets are corresponding schematics. (**D**) Output intensity of lasing emission as a function of the pumped energy, where we used CLC capsules with five different FRs in (C). (**E**) Output intensity relative to the input energy on the flattened area of capsules (left *x* axis) for a pumped energy of 1.4 μJ per pulse, where we normalized the value by that of a spherical capsule (FR = 0). We also included the FWHM of emission spectra above the threshold energy (right *y* axis).

Shape-reconfigurable resonator

The CLC capsules are reversibly deformable so that they can fit into various geometries. For example, we can insert the capsule into a polygonal hole to transform the shape (Fig. 4A). The polygonal holes are designed in a polydimethylsiloxane (PDMS) film to fully accommodate the capsule volume. For this, we determined the lateral dimension of each polygonal hole to have an opening area corresponding to 70% of the projection area of the capsules, and we set the height to 250 μm; the diameter of capsules is 207 μm. When the capsules are pressurized and inserted into the holes, they are deformed by adopting the confining geometries. During the deformation, the inner liquid shell remains unruptured, enabling the planar alignment of LC molecules along the interface of the core.

The deformation of the capsules leads to the formation of new defects. When the CLC is contained in a spherical capsule, a planar alignment along the spherical interfaces makes the helical axes radially oriented, thereby resulting in a point defect in the origin of the sphere. The capsules in the polygonal holes maintain the planar alignment along the deformed surfaces. As the capsules are not in contact with a solid wall along the hole axis, the top and bottom surfaces remain curved, which makes helical axes radially oriented in each part. Therefore, the capsules show a small reflection dot in the centermost (Fig. 4A). At the same time, the capsules are flattened on the side walls, which leads to the formation of line defects along the diagonal directions from the center. The LC molecules are aligned parallel to the flattened side walls in the presence of the alignment layer, and therefore, helical axes are aligned perpendicularly. Therefore, the line defects are formed along the diagonal boundaries at which two neighboring domains with different orientations meet. We observed line defects at the central area of capsules confined in triangular, square, and pentagonal holes. As the capsules are not sharply folded but smoothly curved at the corners of the polygonal holes, the line defects do not span the entire diagonals from the center to the vertices. In the hexagonal holes, capsule does not show line defects as the container with a large corner angle insignificantly deviates from the spherical capsule.

We can use the capsules confined in the polygonal holes for lasing. We expect lasing to occur along the perpendicular directions to top, bottom, and flattened side surfaces. We estimated the threshold energy at 0.98 μJ per pulse for the lasing from the top surface of capsule confined in a square hole and the FWHM of the emission to be 0.63 nm (Fig. 4C). The threshold energy and FWHM are comparable with those from spherical capsules, indicating that the deformation does not degrade the structural quality of resonator as the alignment

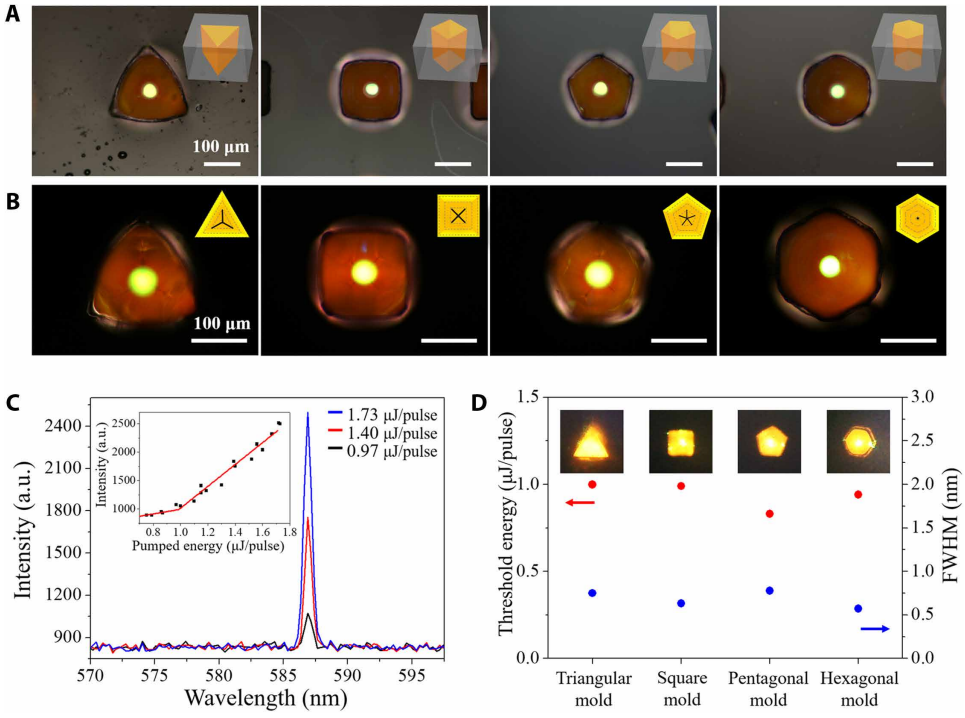

Fig. 4. Shape-reconfigurable capsule resonators. (**A** and **B**) OM images of CLC capsules inserted in polygonal holes taken in reflection mode without polarization (A) and with cross-polarization (B). The insets of (A) show a shape of polygonal holes, and the insets of (B) are schematics for planar alignment of CLC (dotted lines) and line defects (solid lines). (**C**) Series of the emission spectra from the capsule confined in the square hole at various pumped energies. The inset shows a threshold behavior of the emission, where the threshold value is 0.98 μJ per pulse. (**D**) Threshold energy (red circles; left *y* axis) and FWHM of laser spectra (blue circles; right *y* axis) for the capsules confined in the triangular, square, pentagonal, and hexagonal holes. Insets show lasing from the shape-transformed capsules.

shell fully covers the CLC in the core. The threshold and FWHM are also consistent for all the polygonal capsules (Fig. 4D). Therefore, we can use the CLC capsule as shape-reconfigurable resonators that enable the control over lasing direction and intensity.

DISCUSSION

Here, we design shape-reconfigurable photonic capsules containing CLC and use them as an air-stable, wavelength-tunable, and direction-controllable laser resonator. As the dye-dissolved CLC is fully enclosed by an aqueous alignment inner shell, a planar alignment of LC molecules along the interface is maintained. In addition, the elastic outer shell protects the CLC and alignment shell from the surrounding environment. Therefore, the photonic capsules are stable in an air environment and provide omnidirectional lasing even in the absence of any liquid medium. Moreover, one can formulate the fluidic CLC in the core of the capsule to have a temperature-sensitive stop band, which enables the fine-tuning of laser wavelength through temperature control. The high flexibility of the elastic outer shell renders the capsule shape-reconfigurable so that the capsules can be deformed into the disk and polygonal shapes. In particular, the thin shell of the liquid alignment layer maintains its integrity during the dynamic deformation, ensuring the planar alignment and perpendicular arrangement of helical axes. Therefore, one can adjust a lasing direction from omnidirectional to bi- or multidirectional, depending on the shape of the capsules. Moreover, the laser intensity is also controllable as the lasing direction sets the intensity to the target location. This capsule-type resonator can be injected, suspended, and implanted into target volumes. Therefore, we believe that the capsule resonators potentially serve as microlasers for localized irradiation in various chemical and biomedical applications.

MATERIALS AND METHODS

Materials

A temperature-insensitive CLC solution was prepared by mixing nematic LC (E7, Merck) with 2.64% (w/w) of a right-handed chiral dopant (R5011, HCCH). A temperature-responsive CLC solution was formulated by mixing the LC with two right-handed chiral dopants of 19.8% (w/w) of R811 (Merck) and 0.68% (w/w) of R5011. As a gain medium, 0.5% (w/w) of fluorescent dye of PM597 [1,3,5,7,8-pentamethyl-2,6-di-t-butylpyrromethene-difluoroborate complex (TCI)] was doped into the CLC mixtures. The aqueous alignment shell was an aqueous solution of 12% (w/w) of PVA (M_w, 13,000 to 23,000; 87 to 89% hydrolyzed; Sigma-Aldrich) and 7% (w/w) of glycerol (Sigma-Aldrich). The continuous phase was an aqueous solution of 10% (w/w) of PVA. The outer-shell phase was silicone methacrylate monomer (SB4722, Evonik Industries) containing 1% (w/w) of photoinitiator (2-hydroxy-2-methylpropiophenone, Sigma-Aldrich).

Preparation of CLC capsules

A capillary microfluidic device comprised two tapered cylindrical glass capillaries coaxially assembled in a square capillary (fig. S1). The cylindrical capillaries were tapered by a puller (P-97, Sutter Instrument) and sanded to have a diameter of either 200 or 280 μm.

The inner wall of the cylindrical capillary with a 200-μm orifice was first treated with 2-[methoxy(polyethyleneoxy)propyl] trimethoxy silane (Gelest Inc.) to render the surface hydrophilic, and then, the outer wall was treated with trimethoxy(octadecyl)silane (Sigma-Aldrich) to render the surface hydrophobic. The whole surfaces of the capillary with a 280-μm orifice were treated with 2-[methoxy(polyethyleneoxy)propyl] trimethoxy silane (Gelest Inc.) to render them hydrophilic. Afterward, two cylindrical capillaries were coaxially assembled in the square capillary to have a tip-to-tip alignment with a separation of 200 μm. The innermost CLC solution and an aqueous solution for the inner shell were simultaneously injected through the cylindrical capillary with the 200-μm orifice, and the silicone monomer for the outer shell was injected through the interstice between the cylindrical and square capillaries. At the same time, the continuous phase was injected through the interstice between the cylindrical capillary with the 280-μm orifice and square capillary as a counterflow. Flow rates of the four fluids were typically set to 120, 200, 300, and 3200 μl hour^{-1} from the innermost to the continuous phase using syringe pumps (KD Scientific Inc.). The formation of triple-emulsion drops was observed with an optical microscope (TS100, Nikon) equipped with a high-speed camera (MotionScope M3, Redlake). The outer shell was polymerized by irradiating the droplets with UV (CoolWave UV Curing System, Nordson) for 2 min after collecting the drops. The resulting capsules were suspended in the aqueous solution of 5% (w/w) of PVA and 4% (w/w) of glycerol, which leads to the floatation of CLC-loaded capsules made from the triple-emulsion drops and the sedimentation of CLC-free capsules from the double-emulsion drops due to the difference in average density.

Preparation of PDMS mold

The PDMS molds were prepared by soft lithography. To make master molds, an SU-8 100 (MicroChem) was spin-coated on plasma-treated silicon water at 1000 rpm, which resulted in a 250-μm-thick layer after prebaking. The SU-8 film was subjected to photolithography with photomasks with transparent windows of triangular, square, pentagonal, and hexagonal shapes. The lateral dimensions of the polygons were 230, 150, 120, and 100 μm, respectively. Resulting polygonal pillars were replicated to polygonal holes in PDMS by pouring and curing the mixture of a PDMS prepolymer (Slygard 184, Dow Corning) and cross-linker in a 10:1 weight ratio on them.

Characterization

The CLC capsules were observed by optical microscopy in a reflection mode (L150, Nikon) and a transmission mode (Ti-U, Nikon) with a cross-polarizing filter. The reflection spectra were measured using a fiber-coupled spectrometer (USB 4000, Ocean Optics) mounted on a microscope (L150, Nikon) with a 50× lens [numerical aperture (NA), 0.80] for the capsules and 20× lens (NA, 0.45) for CLC films, where a field stop was used to measure the spectrum from the top surface of the capsules. For dye-dissolved CLCs, the reflectance spectra were obtained by subtracting the spectrum taken at 60°C (isotropic state) from the measured one. The capsules were optically pumped by Q-switched double Nd:YAG laser with a pulse duration of 4 ns, a repetition rate of 1 Hz (Brio, Quantel), and a beam diameter of 800 μm. The energy of the pumping source was measured by an energy meter (843-R, Newport) coupled with a pyroelectric energy sensor (919E series, Newport), and the emission spectra from the capsules were measured using the fiber-coupled spectrometer with an optical resolution of 0.5 nm (FWHM, measured $\Delta\lambda \sim 0.25$ nm). The FWHM values of the emission spectra were estimated by fitting with a Gaussian function. A spontaneous emission spectrum of the dye was measured by heating the dye-dissolved CLC solution to 60°C at which LC was in an isotropic state. The optically pumped capsules were observed with a portable scope equipped with a complementary metal-oxide semiconductor image sensor (Smart Scope, SK telecom). To study the influence of temperature on lasing wavelength, a temperature-controllable stage (LTS120, Linkam) was used.

SUPPLEMENTARY MATERIALS

Supplementary material for this article is available at http://advances.sciencemag.org/cgi/content/full/4/6/eaat8276/DC1

section S1. Microfluidic production of triple-emulsion drops
section S2. Photonic cross-communication in CLC capsule array
section S3. Optical setup for measurement of emission from CLC capsules
section S4. Temperature dependence of photonic stop-band of CLC solution
section S5. Competition between SWE and LWE
section S6. Temperature-dependent threshold energy
section S7. Input energy on the flattened area of deformed capsule
section S8. Enhancement of lasing intensity and reduction of FWHM during incubation
fig. S1. Preparation of triple-emulsion drops using a capillary microfluidic device.
fig. S2. Photonic cross-communication.
fig. S3. Optical setup for emission measurement from capsules.
fig. S4. Tuning of photonic stop band with temperature.
fig. S5. Competition between SWE and LWE for lasing.
fig. S6. Temperature-dependent threshold energy.
fig. S7. Input energy on the flattened area of deformed capsule.
fig. S8. Enhancement of laser quality over incubation.
movie S1. Spontaneous healing of oily streak in deformed capsule.

REFERENCES AND NOTES

1. V. I. Kopp, B. Fan, H. K. M. Vithana, A. Z. Genack, Low-threshold lasing at the edge of a photonic stop band in cholesteric liquid crystals. *Opt. Lett.* **23**, 1707–1709 (1998).
2. M. Mitov, Cholesteric liquid crystals with a broad light reflection band. *Adv. Mater.* **24**, 6260–6276 (2012).
3. Y. Matsuhisa, Y. Huang, Y. Zhou, S.-T. Wu, R. Ozaki, Y. Takao, A. Fujii, M. Ozaki, Low-threshold and high efficiency lasing upon band-edge excitation in a cholesteric liquid crystal. *Appl. Phys. Lett.* **90**, 091114 (2007).
4. A. H. Gevorgyan, K. B. Oganesyan, R. V. Karapetyan, M. S. Rafayelyan, The photonic density of states and the light energy density in cholesteric liquid crystal cells. *Laser Phys. Lett.* **10**, 125802 (2013).
5. T. Matsui, R. Ozaki, K. Funamoto, M. Ozaki, K. Yoshino, Flexible mirrorless laser based on a free-standing film of photopolymerized cholesteric liquid crystal. *Appl. Phys. Lett.* **81**, 3741–3743 (2002).
6. J. Schmidtke, W. Stille, H. Finkelmann, S. T. Kim, Laser emission in a dye doped cholesteric. *Adv. Mater.* **14**, 746–749 (2002).
7. A. D. Ford, S. M. Morris, H. J. Coles, Photonics and lasing in liquid crystals. *Mater. Today* **9**, 36–42 (2006).
8. J. P. Dowling, M. Scalora, M. J. Bloemer, C. M. Bowden, The photonic band edge laser: A new approach to gain enhancement. *J. Appl. Phys.* **75**, 1896–1899 (1994).
9. H. Coles, S. Morris, Liquid-crystal lasers. *Nat. Photonics* **4**, 676–685 (2010).
10. J. Xiang, A. Varanytsia, F. Minkowski, D. A. Paterson, J. M. D. Storey, C. T. Imrie, O. D. Lavrentovich, P. Palffy-Muhoray, Electrically tunable laser based on oblique heliconical cholesteric liquid crystal. *Proc. Natl. Acad. Sci. U.S.A.* **113**, 12925–12928 (2016).
11. H. Finkelmann, S. T. Kim, A. Muñoz, P. Palffy-Muhoray, B. Taheri, Tunable mirrorless lasing in cholesteric liquid crystalline elastomers. *Adv. Mater.* **13**, 1069–1072 (2001).
12. L.-J. Chen, J.-D. Lin, S.-Y. Huang, T.-S. Mo, C.-R. Lee, Thermally and electrically tunable lasing emission and amplified spontaneous emission in a composite of inorganic quantum dot nanocrystals and organic cholesteric liquid crystals. *Adv. Opt. Mater.* **1**, 637–643 (2013).
13. L. Chen, Y. Li, J. Fan, H. K. Bisoyi, D. A. Weitz, Q. Li, Photoresponsive monodisperse cholesteric liquid crystalline microshells for tunable omnidirectional lasing enabled by a visible light-driven chiral molecular switch. *Adv. Opt. Mater.* **2**, 845–848 (2014).
14. S.-T. Hur, B. R. Lee, M.-J. Gim, K.-W. Park, M. H. Song, S.-W. Choi, Liquid-crystalline blue phase laser with widely tunable wavelength. *Adv. Mater.* **25**, 3002–3006 (2013).

15. T. Manabe, K. Sonoyama, Y. Takanishi, K. Ishikawa, H. Takezoe, Toward practical application of cholesteric liquid crystals to tunable lasers. *J. Mater. Chem.* **18**, 3040–3043 (2008).
16. J. Schmidtke, W. Stille, Fluorescence of a dye-doped cholesteric liquid crystal film in the region of the stop band: Theory and experiment. *Eur. Phys. J. B.* **31**, 179–194 (2003).
17. S. M. Morris, P. J. W. Hands, S. Findeisen-Tandel, R. H. Cole, T. D. Wilkinson, H. J. Coles, Polychromatic liquid crystal laser arrays towards display applications. *Opt. Express* **16**, 18827–18837 (2008).
18. P. J. W. Hands, S. M. Morris, T. D. Wilkinson, H. J. Coles, Two-dimensional liquid crystal laser array. *Opt. Lett.* **33**, 515–517 (2008).
19. M. Humar, I. Muševič, 3D microlasers from self-assembled cholesteric liquid-crystal microdroplets. *Opt. Express* **18**, 26995–27003 (2010).
20. L.-J. Chen, L.-L. Gong, Y.-L. Lin, X.-Y. Jin, H.-Y. Li, S.-S. Li, K.-J. Che, Z.-P. Cai, C. J. Yang, Lab on a Chip Microfluidic fabrication of cholesteric liquid crystal core-shell structures toward magnetically transportable microlasers. *Lab Chip* **16**, 1206–1213 (2016).
21. P.-. Sun, Z. Liu, W. Wang, X. Wang, H.-m. Zhang, Y.-x. Lu, W. Hu, Y. Lu, D. Shen, Z.-g. Zheng, Lasing of self-organized helical cholesteric liquid crystal micro-droplets based on emulsification. *Opt. Mater. Express* **6**, 1256–1261 (2016).
22. B. Schwarz, Lidar: Mapping the world in 3D. *Nat. Photonics* **4**, 429–430 (2010).
23. T. J. Allen, O. Ogunlade, E. Zhang, P. C. Beard, Large area laser scanning optical resolution photoacoustic microscopy using a fibre optic sensor. *Biomed. Opt. Express* **9**, 650–660 (2018).
24. F. Zhou, B. Peng, Y. Cui, Y. Wang, H. Tan, A novel laser vision sensor for omnidirectional 3D measurement. *Opt. Laser Technol.* **45**, 1–12 (2013).
25. G. Cipparrone, A. Mazzulla, A. Pane, R. J. Hernandez, R. Bartolino, Chiral self-assembled solid microspheres: A novel multifunctional microphotonic device. *Adv. Mater.* **23**, 5773–5778 (2011).
26. S. S. Lee, S. K. Kim, J. C. Won, Y. H. Kim, S.-H. Kim, Reconfigurable photonic capsules containing cholesteric liquid crystals with planar alignment. *Angew. Chem. Int. Ed.* **54**, 15266–15270 (2015).
27. J. Noh, K. Reguengo De Sousa, J. P. F. Lagerwall, Influence of interface stabilisers and surrounding aqueous phases on nematic liquid crystal shells. *Soft Matter* **12**, 367–372 (2016).
28. J. Noh, H.-L. Liang, I. Drevensek-Olenik, J. P. F. Lagerwall, Tuneable multicoloured patterns from photonic cross-communication between cholesteric liquid crystal droplets. *J. Mater. Chem. C* **2**, 806–810 (2014).
29. S. S. Lee, H. J. Seo, Y. H. Kim, S.-Y. Kim, Structural color palettes of core–shell photonic ink capsules containing cholesteric liquid crystals. *Adv. Mater.* **29**, 1606894 (2017).
30. J. Fan, Y. Li, H. K. Bisoyi, R. S. Zola, D.-. Yang, T. J. Bunning, D. A. Weitz, Q. Li, Light-directing omnidirectional circularly polarized reflection from liquid-crystal droplets. *Angew. Chem. Int. Ed.* **54**, 2160–2164 (2015).
31. G. Tkachenko, E. Brasselet, Optofluidic sorting of material chirality by chiral light. *Nat. Commun.* **5**, 3577 (2014).
32. Y. Zhou, Y. Huang, S.-T. Wu, Enhancing cholesteric liquid crystal laser performance using a cholesteric reflector. *Opt. Express* **14**, 3906–3916 (2006).
33. S.-Y. T. Tzeng, C.-N. Chen, Y. Tzeng, Thermal tuning band gap in cholesteric liquid crystals. *Liq. Cryst.* **37**, 1221–1224 (2010).
34. K. S. Shim, J. U. Heo, S. I. Jo, Y.-J. Lee, H.-R. Kim, J.-H. Kim, C.-J. Yu, Temperature-independent pitch invariance in cholesteric liquid crystal. *Opt. Express* **22**, 15467–15472 (2014).
35. M.-Y. Jeong, K. Kwak, Active thermal fine laser tuning in a broad spectral range and optical properties of cholesteric liquid crystal. *Appl. Opt.* **55**, 9378–9383 (2016).
36. S. M. Morris, A. D. Ford, M. N. Pivnenko, H. J. Coles, Enhanced emission from liquid-crystal lasers. *J. Appl. Phys.* **97**, 023103 (2005).
37. C. Mowatt, S. M. Morris, M. H. Song, T. D. Wilkinson, R. H. Friend, H. J. Coles, Comparison of the performance of photonic band-edge liquid crystal lasers using different dyes as the gain medium. *J. Appl. Phys.* **107**, 043101 (2010).
38. F. Araoka, K.-C. Shin, Y. Takanishi, K. Ishikawa, H. Takezoe, Z. Zhu, T. M. Swager, How doping a cholesteric liquid crystal with polymeric dye improves an order parameter and makes possible low threshold lasing. *J. Appl. Phys.* **94**, 279–283 (2003).
39. P. G. Kim, H. A. Stone, Dynamics of the formation of antibubbles. *Europhys. Lett.* **83**, 54001 (2008).

Acknowledgments: We thank M. H. Song and B. R. Lee in Ulsan National Institute of Science and Technology for the help with preliminary measurement of emission spectra. **Funding:** This work was supported by the Mid-Career Researcher Program (NRF-2017R1A2A2A05001156), X-project (NRF-2017R1E1A2A02066688), and the Global Frontier Research Program (2015M3A6A5065315) through NRF grants funded by the Ministry of Science, ICT and Future Planning. **Author contributions:** S.S.L. carried out the overall experiments. J.B.K. helped with the preparation of the PDMS mold. S.S.L., Y.H.K., and S.-H.K. designed the project. S.S.L. and S.-H.K. wrote the manuscript. **Competing interests:** The authors declare that they have no competing interests. **Data and materials availability:** All data needed to evaluate the conclusions in the paper are present in the paper and/or the Supplementary Materials. Additional data related to this paper may be requested from the authors.

Submitted 10 April 2018
Accepted 10 May 2018
Published 22 June 2018
10.1126/sciadv.aat8276

Citation: S. S. Lee, J. B. Kim, Y. H. Kim, S.-H. Kim, Wavelength-tunable and shape-reconfigurable photonic capsule resonators containing cholesteric liquid crystals. *Sci. Adv.* **4**, eaat8276 (2018).

Science Advances

Wavelength-tunable and shape-reconfigurable photonic capsule resonators containing cholesteric liquid crystals

Sang Seok Lee, Jong Bin Kim, Yun Ho Kim and Shin-Hyun Kim

Sci Adv **4** (6), eaat8276.
DOI: 10.1126/sciadv.aat8276